Human Gait Acquisition and Characterization

João P. Ferreira, Manuel M. Crisóstomo, and A. Paulo Coimbra, *Member, IEEE*

Abstract—This paper analyzes human motion, more specifically the human gait in the sagittal plane. A video camera is used to acquire images of a walking person, fitted with a set of white light-emitting diodes (LEDs). The acquired trajectories of the light points are then used to specify joint trajectories in a biped robot. To analyze the stability of the human gait, a system was also developed to acquire the center of pressure (CoP). This system uses eight force sensors, four under each foot. The influence of the human torso angle on the CoP position during walking was confirmed. Some experiments were carried out on a biped robot, and the results show that the acquired human gait can be used in a biped robot, after scale conversion.

Index Terms—Biped robotics, force sensor, human gait, image processing, sagittal balance.

I. INTRODUCTION

INTEGRATING humans and robotic machines into a single system offers multiple opportunities for creating assistive technologies that can be used in biomedical, industrial, and aerospace applications. A human's ability to perform physical tasks is limited not by intelligence but by physical strength and precision, whereas robotic machines can easily carry out rigorous tasks such as maneuvering heavy objects; at the same time, current artificial control algorithms that govern robots, although highly developed, still cannot achieve the comparable performance of naturally developed algorithms used by humans.

The study of the human gait has generated much interest in fields like biomechanics, robotics, and computer animation. It has been studied in medical science [1]–[3], psychology [4], [5], and biomechanics [6]–[8] for five decades. Recognizing humans by their gait has recently been investigated in computer vision.

In biometric terms, human gait may be defined as a means of identifying individuals by the way they walk [9]. Human gait is a pattern of human locomotion and can be described by kinetic or kinematic characteristics [10]. Gait signatures are the most

J. P. Ferreira is with the Institute of Systems and Robotics, Department of Electrical and Computer Engineering, University of Coimbra, 3030-290 Coimbra, Portugal, and also with the Department of Electrical Engineering, Instituto Superior de Engenharia de Coimbra, 3030-199 Coimbra, Portugal (e-mail: ferreira@mail.isec.pt).

M. M. Crisóstomo and A. P. Coimbra are with the Institute of Systems and Robotics, Department of Electrical and Computer Engineering, University of Coimbra, 3030-290 Coimbra, Portugal (e-mail: mcris@isr.uc.pt; acoimbra@deec.uc.pt).

effective and well-defined representation methods for kinematic gait analysis. They can be extracted by motion information from human gaits, and this is crucial for computer graphics, clinical applications, and human identification.

Studies similar to ours [16] are described in [11]–[13]. They analyze a human gait and compare it with medical data acquired by a marker system. However, using markers needs intrusive and expensive specialized hardware and requires contact with the person. Other studies and results are compiled in [14].

For humanoid robotics, stable static walking is when the projection of the center of mass (CoM) on the floor always lies inside the support polygon. The support polygon corresponds to the support foot in the single-support phase, if there is flat contact with the ground. In the double-support phase, the support polygon is formed by the convex polygon inscribing the two feet. In static walking, the robot is always in a static equilibrium, so it can stop its motion at any moment and not fall down. Note that fast motions are not possible, since the dynamic couplings of the body parts could affect the static equilibrium.

The center of pressure (CoP) is defined as the point on the ground where the resultant of the ground-reaction forces acts. In a static stable gait, the CoP and the CoM projection coincide.

In stable dynamic walking, the projection of the CoM on the floor is outside of the supporting polygon during some phases of the gait. The zero-moment point (ZMP), however, is always inside the support polygon. The ZMP is the point where the sum of all forces and moments is zero and is useful for calculating the effects of the dynamic forces (e.g., Coriolis, inertia, gravity, and centrifugal) during robot motion. The equilibrium of a robot depends on the overall dynamics, and in general, the motions performed are faster and smoother. The problem is the complexity of the control structure, since it has to include the dynamic model. Vukobratović *et al.* state that theoretical work on the difference between static and dynamic biped postures is still to be done [17].

In a dynamic stable gait, the CoP coincides with the ZMP [17]. In a dynamically unstable gait, the ZMP leaves the supporting polygon, thereby differing from the CoP.

Our paper's aim is to obtain gait signatures using computer vision techniques and to extract kinematic features for describing human motion and equilibrium in the sagittal plane. These results are to be used afterward in the gait specification of biped robots. To achieve this, white light-emitting diodes (LEDs) were located on several points of an individual's body, and images were captured during his locomotion in front of a web cam. Then, using properties of the body parts and guided by anatomical knowledge, the gait characteristics were extracted. A 2-D stick figure is used to represent the human body model, and joint angles are calculated to describe the gait motion.

Results show that this approach works, compared with medical data acquired by a marker system, and proved suitable for the suggested application domains.

Other available techniques for angle trajectory acquisition include the use of 3-D scanners or encoders. Our system is simpler and cheaper than a 3-D scanner and a system based on encoders.

Humanoid gait characterization usually adopts several parameters (for instance, [18] uses five parameters, and [19] uses nine parameters). In this paper, we propose a new normalized biped gait model generator, parameterized with only two variables: step length and leg height. This normalized model, requiring only two parameters, is easily applied to robots and humans with different physical characteristics.

Another objective of this paper is to determine the behavior of the torso movement and its relation to the CoP under each foot of a walking person for static and dynamic gaits. The CoP is obtained by a force sensor acquisition system.

The ZMP reference point in the single-support phase is usually a fixed point on the sole of the supporting foot [20], [24], [25]. However, experiments with walking humans show that the ZMP moves in the single-support phase [21]–[23]. This was confirmed in our experiments, in which the ZMP shifts from the heel to the toe of the supporting foot. We believe that using natural human ZMP reference trajectories for gait generation will result in a more natural and energy-efficient CoM trajectory. In fact, results already reported also show that since the resulting CoM trajectory oscillations are smoother, using nonfixed ZMP trajectories results in more energy-efficient gaits [23].

In this paper, the influence of the time cycle duration on the torso oscillation and on the trajectories of other parts of the body is also analyzed. The behavior of the torso angle movement for different gait steps is also studied.

Some experiments are presented, which demonstrate that the human static walking process is quite different from the dynamic one.

Experiments with a biped robot are also presented, and the results show that using the acquired human gait to control the biped robot is a good alternative to robotic synthesized gaits.

II. HUMAN AND BIPED ROBOT BODY PARTS AND HUMAN GAIT

The human body parts' mean dimensions are related to the height of the person. Fig. 1 shows the body parts' mean dimensions as a percentage of body height H.

Table I lists the average dimension data for each part of the mean human body, each part of the person used in this paper, and each part of the biped robot shown in Fig. 2, as a percentage of their total height. In the case of the biped robot, there is no head, and the pendulum is considered to be its shoulders.

The human body parts' weights (as a percentage of the total weight), obtained from [15], as well as similar data for the biped robot, are presented in Table II.

The joint trajectories of the hip, knee, and foot in the sagittal plane for a single gait cycle of five normal human beings, in five
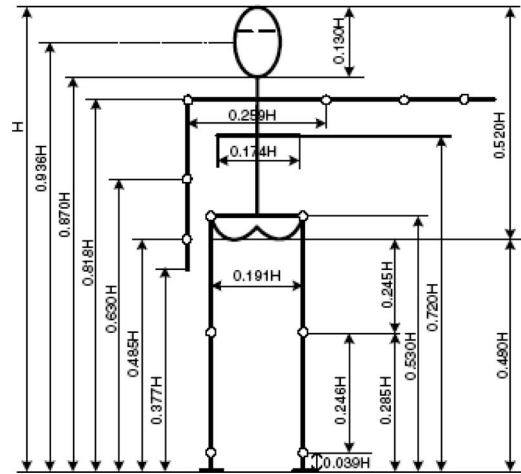

Fig. 1. Human body parts' relative dimensions [7].

TABLE I
HUMAN BODY AND BIPED ROBOT RELATIVE DIMENSION DATA

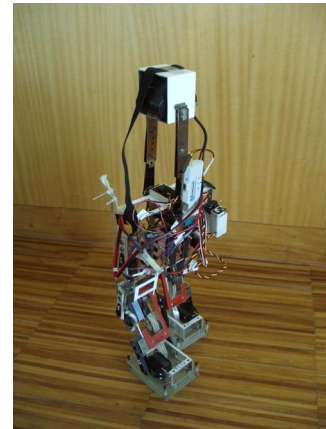| Human Body	Average ratio (%)	Ratio of the person (%)	Biped ratio (%)
Stature	100	100	100
Head to shoulder	19.2	18.6	–
Shoulder to hip	28.8	26	53
Hip to knee	24.5	28	21.2
Knee to ankle	24.6	24.6	21.2
Ankle to sole	3.9	3.8	4.6
Foot length	15.2	14.3	20

Fig. 2. Biped robot used in the experiments.

TABLE II
HUMAN BODY AND BIPED ROBOT WEIGHT DATA

Human Body	Average ratio (%)	Biped ratio (%)
Torso	55.24	23.5
Pelvis	11.0	26.1
Upper leg (thigh)	2×10.35	2×6.5
Lower leg (leg)	2×5.0	2×6.5
Foot	2×1.53	2×12.2

trials each, were presented by Srinivasan and Westervelt [13] and are reproduced in Fig. 3.

The torso joint trajectory and the CoP are also important for the use of human joint trajectories in a robot to provide balance (sagittal stability).
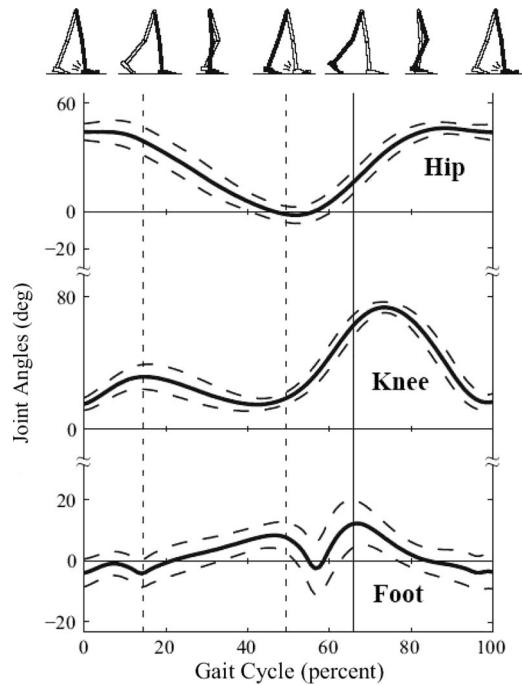
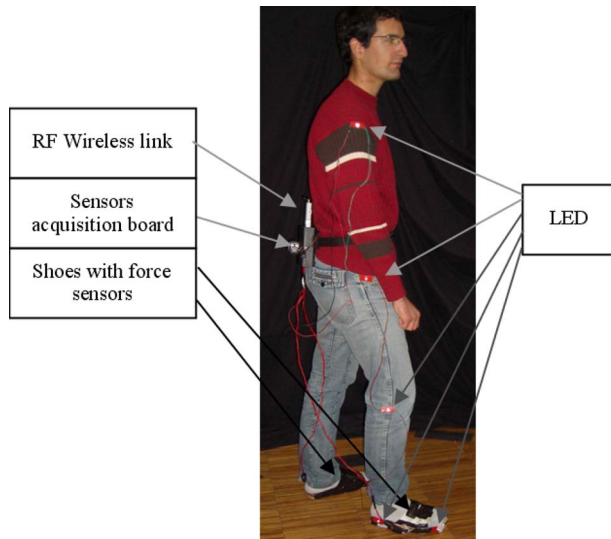Fig. 3. Average joint angles for five persons using five trials each [13].

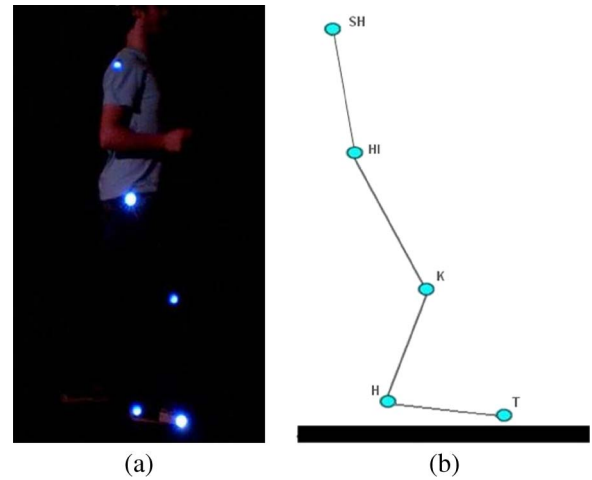Fig. 4. Data acquisition systems in use.

Fig. 5. (a) White LEDs used as marks on the person. (b) Reference points on the person's model.

The tests were carried out using a 26-year-old man, who is 1.85 m tall. To capture the reference marks used on the person, the camera was placed perpendicular to his walking route, 3 m away, and 0.75 m from the floor. This latter distance is half the distance from the floor to the highest reference point, which is the mark on the person's shoulder.

Five reference points (white LEDs) were positioned as shown in Fig. 5(a), forming the five points in Fig. 5(b), where H is the point on the heel, T is the point on the toe of the foot, K is the point on the knee, HI is the point on the hip, and SH is the point on the shoulder.

The distances between the LEDs were also measured, along with the x and z distances between the ankle and the heel. An extra LED on the ankle was thus not necessary.

After the image acquisition of the reference points' trajectories, the angles θ_{SH} (shoulder or torso angle), θ_{HI} (hip angle), θ_K (knee angle), θ_A (ankle angle), and θ_F (foot toe angle), as defined in Fig. 6, were calculated. Point A's coordinates were determined using distance measures taken from the human being.

III. DATA ACQUISITION SYSTEMS

Two data acquisition systems were developed. One uses four force sensors under each foot to determine the CoP; the other is based on computer vision and allows the tracking of five points (white LED marks). Fig. 4 shows the systems fitted on a person.

The first system uses a microprocessor and its 10-bit analog-to-digital converter (ADC) to acquire the force sensor values and to send them to a personal computer via a wireless RS232 transmission link at 9600 b/s.

In the second system, a color web cam was used for the image capture, with the following characteristics: a complimentary metal–oxide–semiconductor 640 × 480 (VGA) sensor, a maximum of 30 frames/s, and a USB 2 interface.

A. Image Acquisition

The image was acquired in red–green–blue (RGB) format. Each RGB image is stored in three 640 × 480 matrices (with 8-bit integers). These three matrices hold the intensity of each pixel for the red, green, and blue primary colors.

Once the images are acquired, implemented software that allows us to obtain all the required information has to be used.

In the first phase, the RGB frame needs to be binarized, being first transformed into an intensity image (gray scale). A threshold level, which is a normalized value of intensity belonging to the interval [0, 1], is then calculated. This threshold is calculated by choosing the level that maximizes the interclass variance of the white and black pixels (by the Otsu method) and is used for the binarization. The threshold level can be increased or decreased if the result obtained is not the one intended.

Fig. 7 shows an image in the RGB format and the result of its binarization, using a 0.8 threshold value.
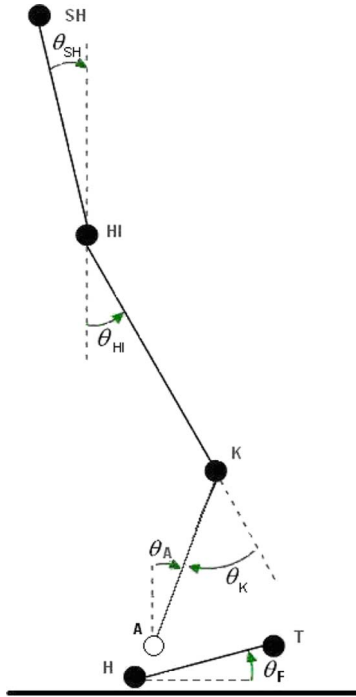
Fig. 6.   Joint angle definitions.

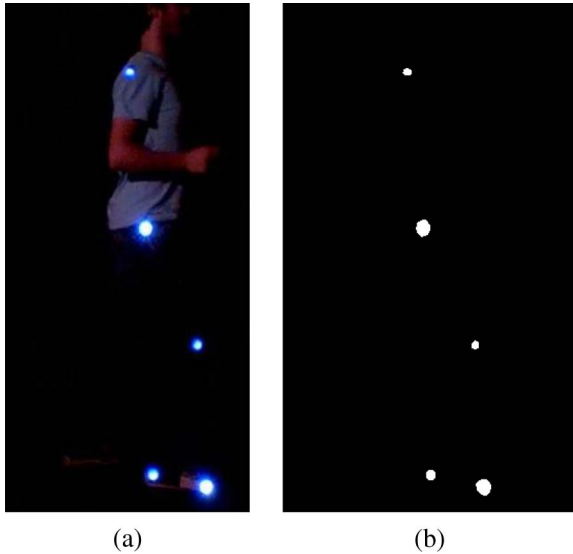(a)   (b)

Fig. 7.   (a) Original acquired image. (b) The result of its binarization.

As can be seen in the binarized image, the objective of isolating the white zones was achieved. A noise filter was used to eliminate small areas of black and white pixels. This phase can be seen as a preprocessing of the image.

After the preprocessing of the captured images, the second phase involved the segmentation of the five white areas (marks). Finally, the CoM of each mark is calculated, and the values of the joint angles are obtained.

B. Force Data System

To determine the CoP, four force sensors are used under each foot (Fig. 8). These sensors are used to measure the
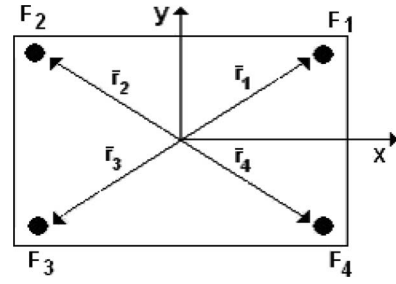

Fig. 8.   Localization of the force sensors in a top view diagram of the foot.

force intensity and where the force is exerted, which is determined by

$$\text{CoP} = \frac{\sum_{i=1}^{8} F_i \cdot \bar{r}_i}{\sum_{i=1}^{8} F_i} \qquad (1)$$

where F_i is the force measured by sensor i, and $\bar{r}_i$ is the position vector.

The force sensor signals are acquired by a 10-bit-resolution ADC with a 30-Hz maximum sampling rate.

The force measurements are noisy, and the force sensors are sensitive to vibrations during the motion, so a second-order Butterworth low-pass filter was used to remove noise and high-frequency vibrations from the force sensors' signals. The difference equation for a second-order low-pass Butterworth digital filter with unity gain has the form

$$y_k = b_1 x_k + b_2 x_{k-1} + b_3 x_{k-2} - a_2 y_{k-1} - a_3 y_{k-2} \qquad (2)$$

where y is the filtered variable, x is the unfiltered variable, x_k is the value of x at time t_k, y_k is the value of y at time t_k, $t_k = k \cdot T$ is the current time, $T = t_k - t_{k-1}$ is the constant sampling interval, and k is an integer.

IV. HUMAN GAIT ANALYZER

A human gait analyzer software application was developed (Fig. 9).

This software application has two operating modes: online and offline.

The online mode allows a continuous image acquisition and its immediate processing and displays both the five joint angles and the position of the light marks placed on the person. It also shows the force in each sensor and the resulting CoP. These data are calculated and displayed every second. This operating mode is used to test the acquisition system, so that the illumination level, the threshold level for image binarization, and the minimum number of pixels for the image of the light from the LED can be set. Only the image areas larger than this minimum are identified as marks (noise filtering).

The offline mode allows a faster image acquisition frame rate (10 frames/s). At the end of the acquisition, the images are saved on disk and processed. The output are the angles of the joints, as defined in Fig. 6, and the position of the light marks
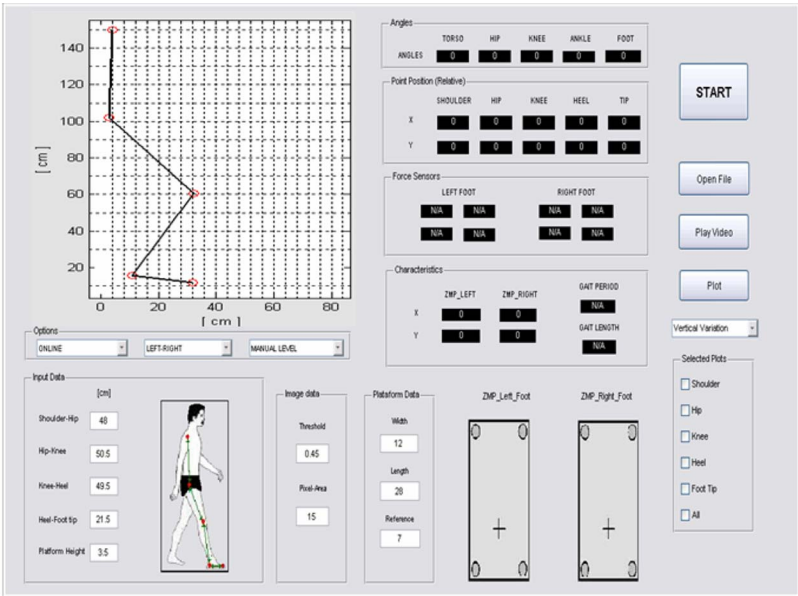
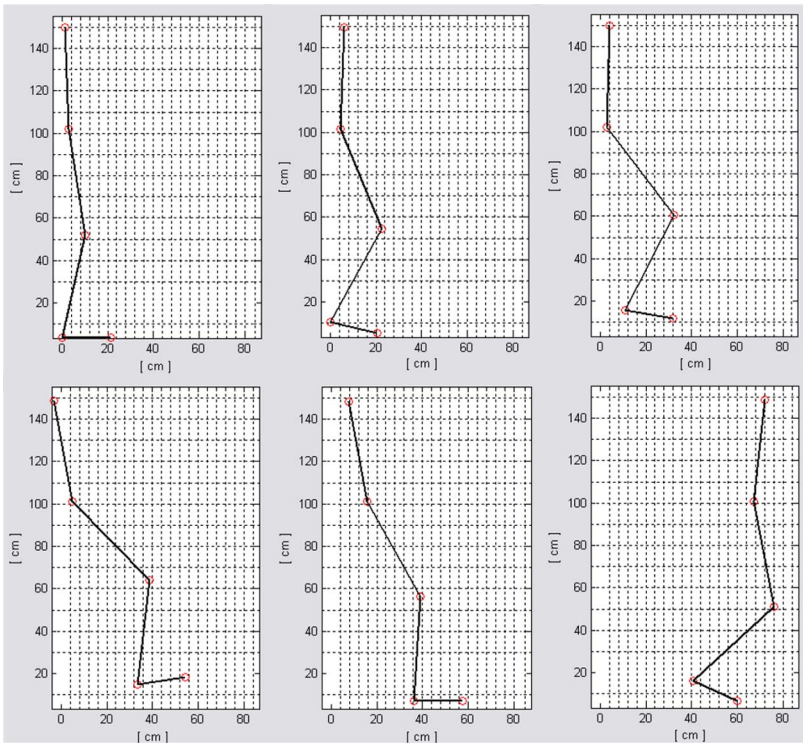Fig. 9.   Human gait analyzer application interface.

Fig. 10.   Human body movement sequence.

placed on the person during the acquisition time, as shown in Fig. 10. This application software also displays on the screen the trajectories of the marks, the trajectories of the joint angles, the force evolution, and the CoP.

All human gait acquisition was performed with the person walking along a plane perpendicular to the web cam's optical axis.

Several tests were carried out to quantify the maximum error of this acquisition method for changes in the direction of motion and changes in the distance to the optical axis.

An LED configuration similar to that in Fig. 7 was attached to a black board. This board was placed in seven locations, in three different directions of motion, and the acquired angles were measured and compared with the real ones. Partial results are shown in Table III.

The distances considered from the web cam's optical axis to the board were 0, 25, 50, 75, −25, −50, and −75 cm. The directions of the movement in front of the camera were the following: one was perpendicular to the web cam's optical axis, and the others were +10° and −10° relative to the previous

TABLE III
ACQUISITION JOINT ANGLE ERRORS

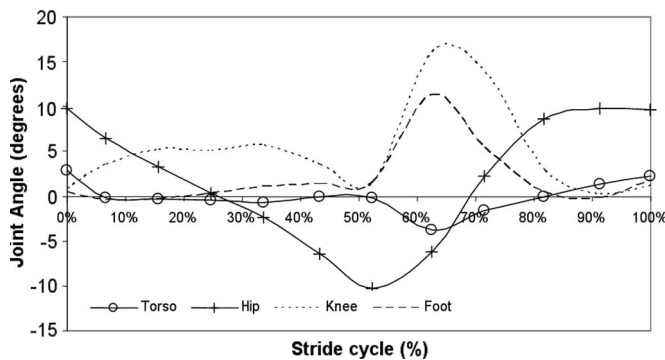| Direction (degrees)	Distance (cm)	Error (degrees)			
		θ_{Torso}	θ_{Hip}	θ_{Knee}	θ_{Foot}
-10	-75	-1.6	0.1	1	-1.4
-10	0	0.2	0	-0.1	-0.3
-10	75	1.1	0.3	-1.3	1.2
0	-75	-0.4	0.6	0.3	**-1.3**
0	0	0	0	0	0
0	75	0.5	-0.5	-0.7	-0.9
10	-75	-0.7	1.2	-1.2	1.4
10	0	0.3	0	-0.2	0.1
10	75	**2**	-1.2	0.6	-0.8

Fig. 11. Joint trajectories of the torso, hip, knee, and foot in the sagittal plane during a single dynamic gait cycle.

direction. In the perpendicular direction (this is the direction walked by the person in the experiments), a maximum error of $1.3°$ was obtained for a 75-cm distance to the optical axis. A maximum error of $2°$ was obtained in the other two directions of movement.

To understand the significance of the above errors, they were compared with the dispersion of the data generated by the same person when repeating similar steps. It was found that the typical dispersion of the hip angles is about $7°$. We can conclude that the acquisition angle errors are smaller than the walking angle variability.

It should also be noticed that for different individuals, the reported results [13] given in Fig. 3 show that the dispersion of the human joint angles is about $10°$.

V. RESULTS

In the first experiment, the trajectories of a 33-cm step length were acquired. This step length (X_{len}) was chosen to maintain the same $X_{\text{len}}/L_{\text{len}}$ ratio of the biped robot, where L_{len} is the leg length.

Results are presented in Figs. 11 and 12, which show the variation of the torso, hip, knee, and foot angles in a gait cycle. Fig. 11 relates to a dynamic gait, and Fig. 12 to a static gait. The cycle times were 2.4 and 8.9 s, respectively.

The profiles obtained for the dynamic behavior are quite similar to those found in the medical literature. It can be seen that the second phase of the step occurred later than that reported by Whittle [1]. The joint angle of the torso was also obtained to see how humans stabilize their gaits.
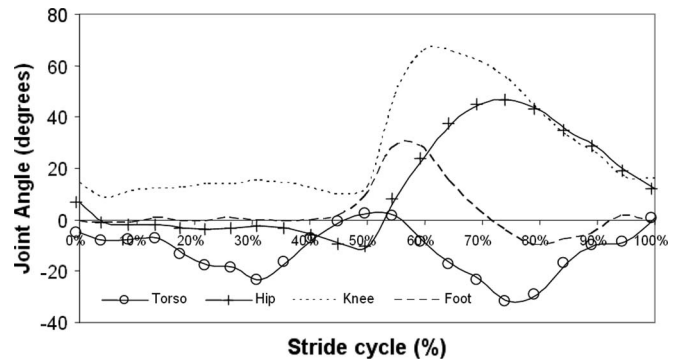

Fig. 12. Joint trajectories of the torso, hip, knee, and foot in the sagittal plane during a single static gait cycle.
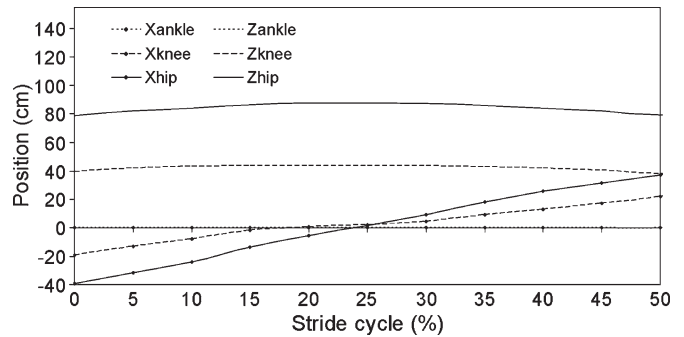

Fig. 13. Trajectories of the hip, knee, and ankle in the sagittal plane during a normal human gait in the first phase of stride.
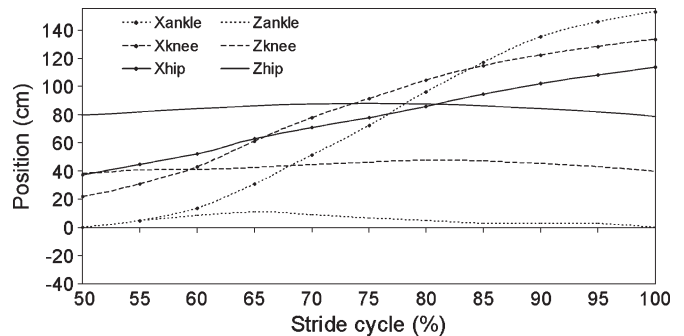

Fig. 14. Trajectories of the hip, knee, and ankle in the sagittal plane during a normal human gait in the second phase of stride.

The values shown in Fig. 12 are smaller than those found in the literature, because the stride used in our tests was 2.3 times shorter. This means that there is a slight difference in the first phase of the gait, since the foot in contact with the floor does not oscillate. In the experiments with the biped robot, its foot always moves parallel to the ground.

In the static gait, there is an increase of the values of the angles in the second phase of the gait. The hip angle is the one that increases most, since larger balance compensation is needed, resulting in a larger torso angle than for the dynamic gait.

Another experiment was performed, consisting of the acquisition of a normal human (150-cm) stride, and the results are presented in the next figures. Figs. 13 and 14 show the Cartesian trajectories of the first and second phase of the stride, respectively, and Fig. 15 shows the joint trajectories.
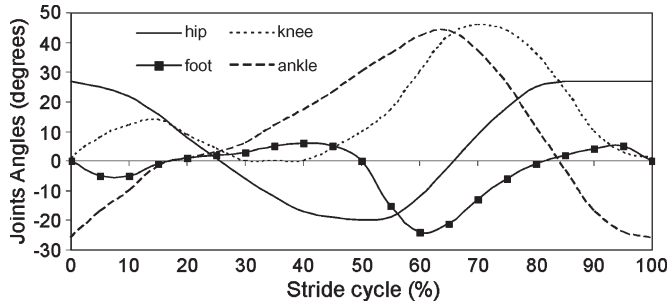
Fig. 15. Joint trajectories of the hip, knee, ankle, and foot in the sagittal plane during a normal human gait.

The behavior of the hip and ankle trajectories [18], [19] is normally used to describe a robotic humanlike gait. The knee trajectory depends on the hip and ankle trajectories.

After finding the Cartesian trajectories of the hip and ankle, the next step was to normalize the points of the hip and ankle trajectories. Applying a polynomial regression to those trajectories, a square coefficient relation of 0.996 was obtained. These trajectories can then be applied to any robot, using the height of the leg (Z_L) and the gait length (X_S) as scale factors. The normalized trajectories are then generated by

$$\begin{bmatrix} X_{\mathrm{hip}} \\ Z_{\mathrm{hip}} \\ X_{\mathrm{ankle}} \\ Z_{\mathrm{ankle}} \end{bmatrix}_{\mathrm{gnd}}^{T} = (A \cdot G_{\mathrm{gnd}})^{T} \cdot XZ_{\mathrm{gnd}} \qquad (3)$$

$$\begin{bmatrix} X_{\mathrm{hip}} \\ Z_{\mathrm{hip}} \\ X_{\mathrm{ankle}} \\ Z_{\mathrm{ankle}} \end{bmatrix}_{\mathrm{mov}}^{T} = (A \cdot G_{\mathrm{mov}})^{T} \cdot XZ_{\mathrm{mov}} \qquad (4)$$

where A is a coefficient polynomial matrix, G_{gnd} is the percentage of the gait cycle vector for the grounded foot, G_{mov} is the percentage of the gait cycle vector for the moving foot, and XZ_{gnd} and XZ_{mov} are scale factor matrices. These matrices
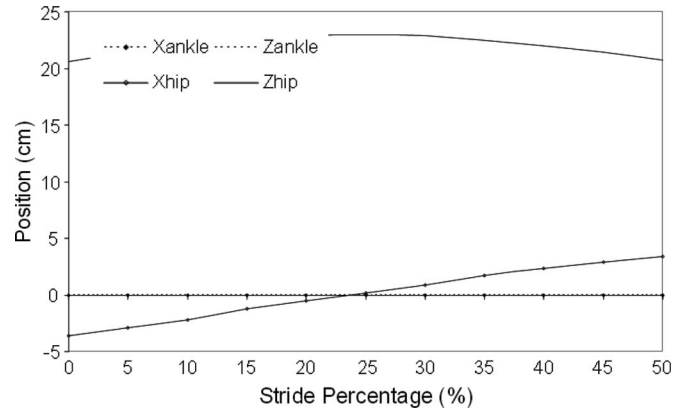

Fig. 16. Robot trajectories of the hip and ankle for the grounded foot (X_{ankle} and Z_{ankle} are zero).

are given by the equations shown at the bottom of the page, where $S_{\%}$ represents the gait cycle percentage and takes values from 0 to 50 in the G_{gnd} vector (grounded foot) and values from 50 to 100 in the G_{mov} vector (moving foot).

In our robot, $Z_L = 23$ cm. For $X_S = 7$ cm, the trajectories of the hip and ankle are shown in Fig. 16 (for the grounded foot) and Fig. 17 (for the moving foot). In the robot movement, the foot always moves parallel to the ground.

To obtain the lateral balance, the pendulum is moved from side to side. The maximum value of the angle of the pendulum ($\theta_{\mathrm{Lateral}}$) was experimentally determined and is constant for all gaits.

Many studies use several parameters to calculate the trajectories of the hip and the ankle, such as A_h, F_h, W_h, and A_a in Fig. 18. Values for these parameters are presented in Table IV for the person in the experiments, whose leg height ($H_{\mathrm{Leg}} = l_1 + l_2$) is 88 cm. For the last row, the gait is considered static. Analyzing these data, it is possible to conclude that in this static gait, weight is transferred in about 41% of the gait cycle. This weight transfer occurs in the double-support phase (when the two feet are in contact with the ground). The single-support

$$A = \begin{bmatrix} 0 & 0 & 0 & 0 & 10.263E{-}03 & 249.033E{-}03 \\ 0 & 0 & 0 & -158.826E{-}06 & 78.736E{-}04 & 897.685E{-}03 \\ 0 & 0 & -15.67E{-}06 & 121.278E{-}05 & -14.623E{-}04 & 26.52E{-}04 \\ -180.869E{-}10 & 208.426E{-}08 & -745.788E{-}07 & 585.999E{-}06 & 954.539E{-}05 & -250.062E{-}06 \end{bmatrix}$$

$$G_{\mathrm{gnd}} = \begin{bmatrix} S_{\%}^{5} \\ S_{\%}^{4} \\ S_{\%}^{3} \\ S_{\%}^{2} \\ S_{\%} \\ 1 \end{bmatrix} \qquad XZ_{\mathrm{gnd}} = \begin{bmatrix} X_S & 0 & 0 & 0 \\ 0 & Z_L & 0 & 0 \\ 0 & 0 & 0 & 0 \\ 0 & 0 & 0 & 0 \end{bmatrix}$$

$$G_{\mathrm{mov}} = \begin{bmatrix} (S_{\%}{-}50)^{5} \\ (S_{\%}{-}50)^{4} \\ (S_{\%}{-}50)^{3} \\ (S_{\%}{-}50)^{2} \\ (S_{\%}{-}50) \\ 1 \end{bmatrix} \qquad XZ_{\mathrm{mov}} = \begin{bmatrix} X_S & 0 & 0 & 0 \\ 0 & Z_L & 0 & 0 \\ 0 & 0 & X_S & 0 \\ 0 & 0 & 0 & Z_L \end{bmatrix}$$
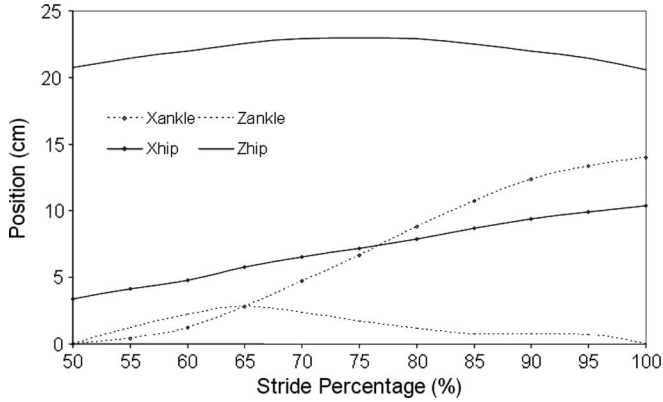
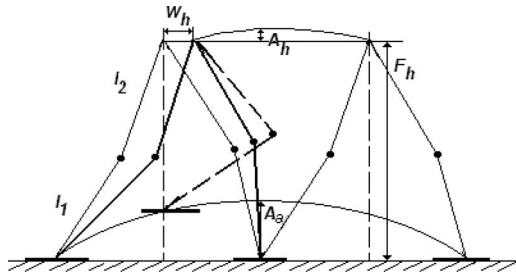Fig. 17.   Robot trajectories of the hip and ankle for the moving foot.

Fig. 18.   Robotic hip and ankle trajectories.

TABLE IV
HUMAN GAIT PARAMETERS

Stride time (s)	A_h (%)	F_h (%)	W_h (%)	A_a (%)
1.4	9.2	90.7	20	12.4
1.9	9.3	90.6	21	12.4
2.7	9.4	90.5	24	12.3
4	9.6	90.3	41	12.1

phase (when only one foot is in contact with the ground) occurs in the remaining time of the gait cycle.

Our tests showed that the value of W_h increases when the walking speed slows and the stride shortens. In the tests with the robot, the value of 41% of the W_h was used to determine the length of time the robot is in the double-support phase.

Two types of trajectory designs were obtained: one using the normalized human gait and another based on the parameters shown in Table IV, normally used in biped robotics.

The behavior of X_{zmp}, $\mathrm{CoP_{left}}$ (CoP of the left foot), $\mathrm{CoP_{right}}$ (CoP of the right foot), and θ_{Torso} during a step cycle of 1.4 s was obtained (see Fig. 19), and some characteristics of human gait balance were found. In each step, the CoP moves from the heel to the toe. Knowing the human trajectory of the CoP makes it possible to design the CoP behavior to be used in the robot.

Analyzing gaits of different persons, it is possible to conclude that humans center their CoP on different points, which are always between the heel and the center of the foot. This implies that the oscillations of the torso have different offsets from person to person.

The amplitudes of the torso oscillations depend on the gait time (see Fig. 20).
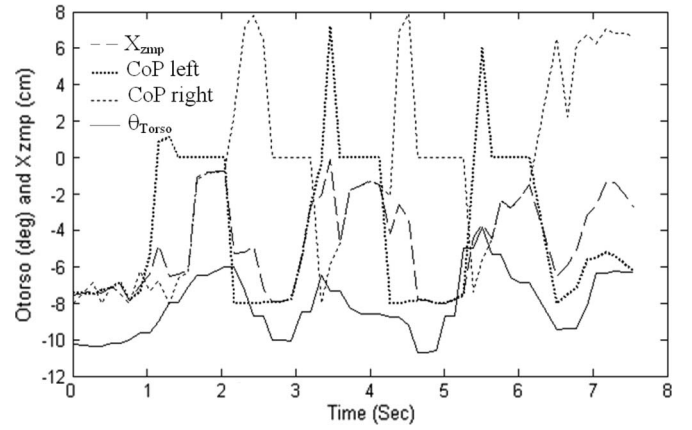
Fig. 19. X_{zmp}, θ_{Torso}, $\mathrm{CoP_{right}}$, and $\mathrm{CoP_{left}}$ of a person walking on a flat surface.
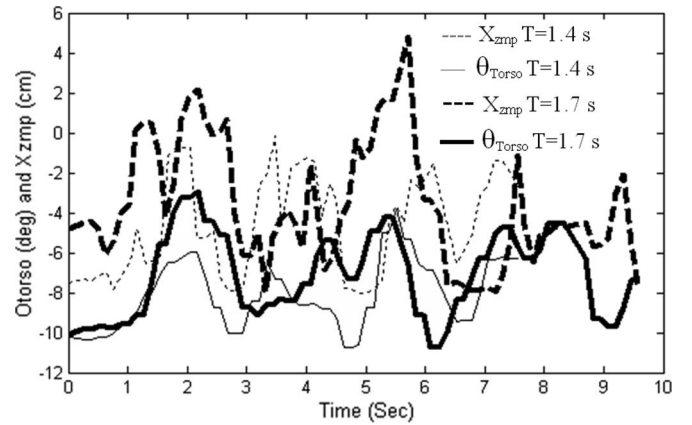
Fig. 20. θ_{Torso} and X_{zmp} of a person walking on a flat surface with step cycles of 1.4 and 1.7 s.

The torso angle in human walking can be approximated by a cosine function, and its maximum value changes with the step cycle. The torso angle model can then be described by

$$\theta_{\mathrm{Torso}} = K(T_{\mathrm{Step}}) \cos \left(\frac{2\,\pi\,S_{\%}}{100} \right) \qquad (5)$$

where $K(T_{\mathrm{Step}})$ is the relationship between the maximum torso oscillation and the step cycle, as shown in Fig. 21, which shows a mean value obtained for seven steps.

Applying a regression, the following expression was obtained:

$$K(T_{\mathrm{Step}}) = 0.2499 \cdot T_{\mathrm{Step}}^2 - 2.5747 \cdot T_{\mathrm{Step}} + 1.092. \qquad (6)$$

Fig. 21 suggests that in this case, the step time limit between static and dynamic human walking is somewhere between 2.5 and 3.5 s. Therefore, it can be concluded that steps taking longer than 3.5 s can be considered as static walking.

VI. APPLICATION OF RESULTS

To determine the functionality of human gaits in the biped robot, two experiments were carried out. Using the trajectories defined in Figs. 16 and 17, obtained by our proposed model,
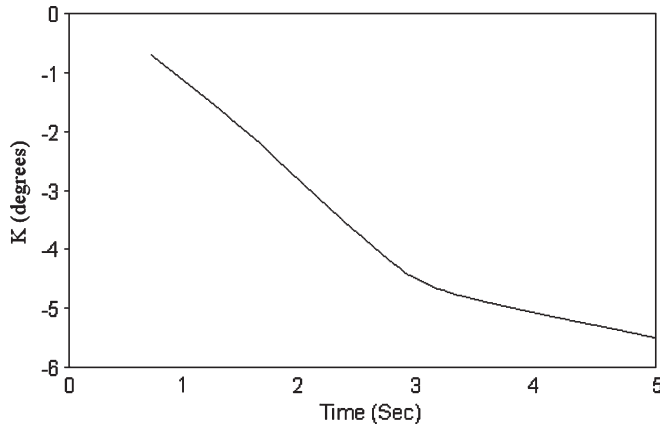
Fig. 21. Relationship between the maximum torso oscillation and the step cycle time.
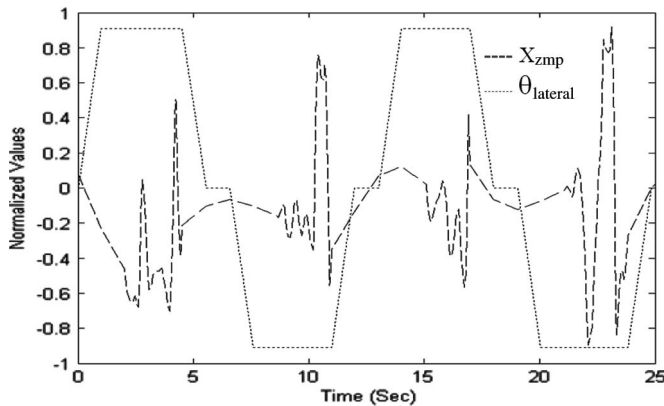

Fig. 22. X_{zmp} and $\theta_{\mathrm{Lateral}}$ of the robot walking on a flat surface and without torso control.

and applying inverse kinematics, the joint angles' trajectories of the legs of the robot were obtained.

In the first experiment, the biped robot was walking on a flat surface, without torso control (the torso was kept vertical). Fig. 22 shows the X_{zmp} behavior acquired by force sensors attached under the robot feet. It can be seen that the X_{zmp} is very irregular and that after some steps, the robot falls. $\theta_{\mathrm{Lateral}}$ is also plotted, allowing the identification of each of the four steps of the experiment. Both X_{zmp} and $\theta_{\mathrm{Lateral}}$ were normalized such that the unit values correspond to 4.7 cm for X_{zmp} and 55° for $\theta_{\mathrm{Lateral}}$.

In the second experiment, the robot was walking on a flat surface with the torso balance control active. Equation (5) was used to obtain the torso angle trajectory. Because the distribution of the mass in the biped robot is different from that in humans, the K to be used in the biped is given by the following equation, which was obtained from a simulation of the biped dynamic model

$$K(T_{\mathrm{Step}}) = 0.002 \cdot T_{\mathrm{Step}}^4 - 0.0637 \cdot T_{\mathrm{Step}}^3$$
$$+ 0.7795 \cdot T_{\mathrm{Step}}^2 - 4.4803 \cdot T_{\mathrm{Step}} + 2.7866. \quad (7)$$

In this experiment, the X_{zmp} behavior was uniform, and the robot walked with stability, as can be seen in Fig. 23, where X_{zmp}, θ_{Torso} and $\theta_{\mathrm{Lateral}}$ were normalized such that the unit
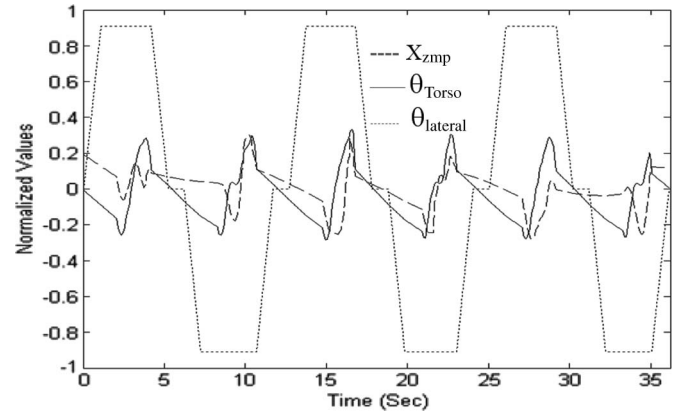

Fig. 23. X_{zmp}, θ_{Torso}, and $\theta_{\mathrm{Lateral}}$ of the robot walking on a flat surface and with torso control.

values correspond to 4.7 cm for X_{zmp}, 25° for θ_{Torso}, and 55° for $\theta_{\mathrm{Lateral}}$.

VII. CONCLUSION AND FUTURE WORK

Analyzing the results, it can be concluded that the objective of acquiring the trajectories of the human gait has been achieved, and a mathematical characterization of human gait has been obtained.

Several tests have been carried out to analyze different gaits of the same person. Using the information obtained, it is possible to identify the characteristics of each gait type.

It can be said that the main objectives have been reached and that the results can be used in the gait definition and balance of biped robots.

The system can be used in medical areas, particularly in diagnosing wear in one ore more joints, by detecting disturbances in a patient's gait.

In the future, human walking on a slope and up and down stairs will be studied, and the results will be applied to a biped robot.

REFERENCES

[1] M. W. Whittle, "Clinical gait analysis: A review," *Hum. Mov. Sci.*, vol. 15, no. 3, pp. 369–387, Jun. 1996.

[2] M. P. Murray, "Gait as a total pattern of movement," *Amer. J. Phys. Med.*, vol. 46, no. 1, pp. 290–333, 1967.

[3] J. Perry, *Gait Analysis: Normal and Pathological Function*. Thorofare, NJ: Slack, 1992.

[4] G. Johansson, "Visual perception of biological motion and a model for its analysis," *Percept. Psychophys.*, vol. 14, no. 2, pp. 201–211, 1973.

[5] S. V. Stevenage, M. S. Nixon, and K. Vince, "Visual analysis of gait as a cue to identity," *Appl. Cogn. Psychol.*, vol. 13, no. 6, pp. 513–526, 1999.

[6] V. T. Inman, H. J. Ralston, and F. Todd, *Human Walking*. Baltimore, MD: Williams & Wilkins, 1981.

[7] D. A. Winter, *The Biomechanics and Motor Control of Human Movement*, 2nd ed. New York: Wiley, 1990.

[8] T. P. Andriacchi and D. E. Hurwitz, "Gait biomechanics and the evolution of total joint replacement," *Gait Posture*, vol. 5, no. 3, pp. 256–264, Jun. 1997.

[9] M. S. Nixon, J. N. Carter, D. Cunado, P. S. Huang, and S. V. Stevenage, "Automatic gait recognition," in *BIOMETRICS—Personal Identification in Networked Society*, A. K. Jain, R. Bolle, and S. Pankanti, Eds. Norwell, MA: Kluwer, 1999, pp. 231–249.

[10] J. K. Aggarwal, Q. Cai, W. Liao, and B. Sabata, "Nonrigid motion analysis: Articulated and elastic motion," *Comput. Vis. Image Underst.*, vol. 70, no. 2, pp. 142–156, May 1998.

[11] M. Nakamura, M. Mori, and J. Nishii, "Trajectory planning for a leg swing during human walking," in *Proc. IEEE Int. Conf. Syst., Man, Cybern.*, 2004, pp. 784–790.

[12] J.-H. Yoo, M. S. Nixon, and C. J. Harris, "Extracting human gait signatures by body segment properties," in *Proc. 5th IEEE SSIAI*, pp. 35–39.

[13] S. Srinivasan and E. R. Westervelt, "An analytically tractable model for a complete gait cycles," in *Proc. 20th Congr. Int. Soc. Biomechanics*, Aug. 2005, p. 795.

[14] *Clinical Gait Analysis Home Page*. [Online]. Available: http://www.univie.ac.at/cga/

[15] A. Seireg and R. Arvikar, *Biomechanical Analysis of the Musculoskeletal Structure for Medicine and Sport*. New York: Hempshire Publishing Co., 1989.

[16] J. P. Ferreira, M. M. Crisóstomo, A. P. Coimbra, D. Carnide, and A. Marto, "A human gait analyzer," in *Proc. IEEE Int. Symp. WISP*, Madrid, Spain, Oct. 3–5, 2007, pp. 1–5.

[17] M. Vukobratović, B. Borovac, and V. Potkonjak, "Towards a unified understanding of basic notions and terms in humanoid biped robotics," *Robotica*, vol. 25, no. 1, pp. 87–101, Jan. 2006.

[18] Q. Huang and Y. Nakamura, "Sensory reflex control for humanoid walking," *IEEE Trans. Robot.*, vol. 21, no. 5, pp. 977–984, Oct. 2005.

[19] F. M. Silva and J. A. T. Machado, "Energy analysis during biped walking," in *Proc. IEEE Int. Conf. Robot. Autom.*, 1999, pp. 59–64.

[20] S. Kajita, F. Kahehiro, K. Kaneko, K. Fujiwara, K. Harada, K. Yokoi, and H. Hirukawa, "Biped walking pattern generation using preview control of the zero-moment-point," in *Proc. IEEE Int. Conf. Robot. Autom.*, Taipei, Taiwan, Sep. 2003, vol. 2, pp. 1620–1626.

[21] A. Dasgupta and Y. Nakamura, "Making feasible walking motion of humanoid robots from human motion capture data," in *Proc. IEEE Int. Conf. Robot. Autom.*, Detroit, MI, May 1999, pp. 1044–1049.

[22] K. Erbatur, A. Okazaki, K. Obiya, T. Takahashi, and A. Kawamura, "A study on the zero moment point measurement for biped walking robots," in *Proc. 7th Int. Workshop Adv. Motion Control*, Maribor, Slovenia, 2002, pp. 431–436.

[23] C. Zhu, Y. Tomizawa, X. Luo, and A. Kawamura, "Biped walking with variable ZMP, frictional constraint, and inverted pendulum model," in *Proc. IEEE Int. Conf. Robot. Biomimetics*, Shenyang, China, Aug. 2004, pp. 425–430.

[24] Y. Choi, B. J. You, and S. R. Oh, "On the stability of indirect ZMP controller for biped robot systems," in *Proc. Int. Conf. Intell. Robots Syst.*, Sendai, Japan, Jun. 2004, vol. 2, pp. 1966–1971.

[25] T. Sugihara, Y. Nakamura, and H. Inoue, "Real-time humanoid motion generation through ZMP manipulation based on inverted pendulum control," in *Proc. IEEE Int. Conf. Robot. Autom.*, Washington, DC, May 2002, vol. 2, pp. 1404–1409.

João P. Ferreira received the B.Sc. degree in electrical engineering and the M.S. degree in industrial automation in 1999 and 2002, respectively, from the University of Coimbra, Coimbra, Portugal, where he is currently working toward the Ph.D. degree.

He is currently a Lecturer with the Department of Electrical Engineering, Instituto Superior de Engenharia de Coimbra, Coimbra, and a Researcher with the Institute of Systems and Robotics, Department of Electrical and Computer Engineering, University of Coimbra. His research interests include biped robots, hyperredundant robots, mobile manipulators, and artificial intelligence and its applications.

Manuel M. Crisóstomo received the B.Sc. degree from the University of Coimbra, Coimbra, Portugal, in 1978, the M.Sc. degree from the Technical University of Lisbon, Lisbon, Portugal, in 1987, and the Ph.D. degree from Brunel University, Uxbridge, U.K., in 1992.

He is currently a Lecturer with the Department of Electrical Engineering and Computer Science, University of Coimbra, where he is also a Researcher with the Institute of Systems and Robotics. His main research interests include robotics, sensors and actuators, and classical and fuzzy control systems.

A. Paulo Coimbra (M'96) received the B.Sc. and Ph.D. degrees in electrical engineering from the University of Coimbra, Coimbra, Portugal, in 1985 and 1996, respectively.

Since 1996, he has been an Assistant Professor with the Department of Electrical and Computer Engineering, University of Coimbra, where he is also a Researcher with the Institute of Systems and Robotics. His research interests include biped robots, hyperredundant robots, and electromagnetic compatibility.